Effects of gamma irradiation on structural, thermal and mechanical properties of polyamide-11/halloysite nanotubes nanocomposites

Mohamed Sahnoune, Mustapha Kaci, Hélène Garay, J. Lopez-Cuesta, Mohamed Mahlous

Effects of gamma irradiation on structural, thermal and mechanical properties of polyamide-11/halloysite nanotubes nanocomposites

Mohamed Sahnoune[1,2], Mustapha Kaci[2], Hélène Garay[3], José-Marie Lopez-Cuesta[3] and Mohamed Mahlous[4]

Abstract

The effect of gamma irradiation on neat Polyamide-11 (PA11) and PA11 filled with 3 wt% of halloysite nanotubes (HNTs) was investigated at various doses up to 100 kGy in air and at room temperature. The irradiation test was conducted on sample films prepared by a twin-screw extruder in the first step then cast extrusion. The study showed the formation of a maximum of gel fraction up to 10 and 20 kGy for neat PA11 and PA11/HNTs, respectively. Furthermore, the results indicated the occurrence of crosslinking at low irradiation dose, whereas chain scission took place at higher ones. Additionally, the results revealed that the presence of HNTs limits the impacts of gamma irradiation through a barrier effect. An optimum irradiation dose was found for thermal and mechanical properties, corresponding to the dose for maximum gel formation. Moreover, experimental design was implemented to highlight the main incidences and interactions of both halloysite incorporation and radiation dose on some relevant effects of gamma irradiation.

[1] Département de Génie des Procédés, Faculté des Sciences et Sciences Appliquées, Université de Bouira, Bouira, Algeria
[2] Laboratoire des Matériaux Polymères Avancés (LMPA), Université de Bejaia, Bejaia, Algeria
[3] Centre des Matériaux des Mines d'Alès (C2MA), IMT Mines d'Alès, Alès cedex, France
[4] Centre de Recherche Nucléaire d'Alger (CRNA), Algiers, Algeria

Corresponding author:
Mohamed Sahnoune, Département de Génie des Procédés, Faculté des Sciences et Sciences Appliquées, Université de Bouira, Bouira 10000, Algeria; Laboratoire des Matériaux Polymères Avancés (LMPA), Université de Bejaia, Béjaïa 06000, Algeria.
Email: m.sahnoune@univ-bouira.dz

Keywords
Gamma irradiation, polyamide-11, halloysite, nanocomposites, degradation

Introduction

Unlike the commonly used polyamide-6 and 6,6, the polyamide-11 (PA11) has the advantage to be biobased and less hydrophilic in addition of its excellent oil resistance. Therefore, PA11 is largely used as green engineering polymer in a wide range of industrial applications from offshore to automotive. PA11 is also biocompatible and so can be used for medical applications or food packaging after appropriate radiation sterilization.[1] However, like other polyamides, PA11 utilization is limited because of its relative low softening point. This shortcoming can be overcome by crosslinking under radiation energy (gamma rays or electron and proton beam).[2,3] Indeed, high-energy radiation causes changes in the chemical and physical properties of the polymer and these changes are due typically to crosslinking and chain scission reactions. The prevalence of one type of reaction over the other, depends on some factors such as the polymer structure, the irradiation atmosphere or the irradiation temperature.[4–8] In this regard, the effects of high-energy radiation on polyamides have been studied intensively since the 1950s.[9–15] The studies showed a considerable increase in carboxyl end groups with the primary effect being crosslinking accompanied with a considerable degradation and loss of crystallinity. However, neither crosslinking nor chain scission, was proportional to the radiation dose.

Halloysite is a clay of kaolin group with the chemical composition $Al_2Si_2O_5(OH)_4.nH_2O$. HNTs possess few hydroxyl groups at their outer surfaces and come mostly in tubular form.[16] This mineral has many advantages such as its biocompatibility, high thermal stability, mechanical reinforcing effect and low cost.[17] These favorable characteristics result in the use of HNTs in a large range of applications. Indeed, several polyamide/halloysite nanocomposite systems were reported in the literature, resulting in an enhancement in tensile properties (Young's modulus, toughness and tensile strength),[18] a lubricant effect,[19] a superior thermal stability,[20] a nucleic effect[21] and a flame-retardant behavior.[22,23] Moreover, halloysite was efficiently used as compatibilizing agent in various polymer ternary nanocomposites.[24–26]

To the best of our knowledge, the literature data is rather scarce on the effect of filler incorporation on gamma irradiation of polyamides. In a first work,[27] it was found that the incorporation of 6–24 wt% of montmorillonite did not affect significantly the evolution of the mechanical properties of irradiated waste polyamide copolymer/waste rubber powder. More recently, Porubská et al.[28] reported that for gamma irradiation of unfilled and glass fibers reinforced PA6, the formation of crosslinked portion was observed in the irradiated materials under inert atmosphere (argon). Whereas, in oxidative atmosphere, gamma irradiation of PA6 and filled PA6 leads as well to an increase in molecular weight but without any formation of crosslink even at highest dose (500 kGy). In addition, the authors reported that gamma irradiation caused only negligible changes in both tensile strength and elongation at break and this with or without the presence of glass fibers.

Therefore, the aim of the present paper is to investigate for the first time the effect of the incorporation of a non-modified nanoclay, in this case halloysite nanotubes, on gamma irradiation in air of PA11. The role of HNTs in PA11 nanocomposite films subjected to gamma irradiation was evaluated through changes in structural, surface, thermal and mechanical properties of the irradiated samples. The structural changes were assessed via Fourier transform infrared spectroscopy as well as contact angle measurements since surface energy can be correlated with the formation of low molecular polar species, especially carbonyls ones, during gamma exposure.

Experimental

Materials

An additives free grade of PA11 (Rilsan® LMNO) was supplied by Arkema (France). The polymer has the following specifications: $\bar{M}_w \approx 51000$ g.mol^{-1} and d = 1.02 g.cm^{-3}. HNTs were extracted from Djebel Debbagh deposit in Guelma (Algeria). The particles have an average diameter of 25 μm and a surface area of 51.4 m^2.g^{-1}. Before processing, HNTs and PA11 pellets were dried under vacuum at 80°C for 24 h and overnight, respectively.

Sample preparation

Virgin PA11 and PA11/HNTs nanocomposite filled at 3 wt% were melt compounded under vacuum using a semi-industrial twin-screw extruder (BC 21 Clextral) at a screw speed of 250 rpm with a screw of diameter (Φ) = 25 mm and length to diameter ratio (L/Φ) = 48. The temperature profile was set at 140/230/235/245/250°C from hopper to die. After pelletizing, the granules were dried under vacuum at 80°C overnight and processed in a cast extrusion machine (HaakeRheomex 19/25 OS, Thermofisher) to obtain films of 0.3 mm thickness. The machine is equipped with a single screw of 25 mm diameter (Φ) and length to diameter ratio (L/Φ) = 25 at a screw speed of rpm. The temperature profile was set at 225/24/235°C from hopper to die.

Gamma irradiation test

Gamma irradiation was carried out on film samples in the form of rectangular bands of 10 × 5 cm^2, in ^{60}Co industrial equipment at the Nuclear Research Center of Algiers. The samples were exposed to 10; 20; 30; 50 and 100 kGy at a dose rate of 1.92 Gy h^{-1} in the presence of air, at room temperature. The codes and compositions of the various formulations used are given in Table 1.

Characterization techniques

Scanning electron microscopy. Scanning electron microscopy (SEM) was used to evaluate the state of dispersion of HNTs in the filled samples. It was conducted under high vacuum with an environmental SEM Quanta 200 FEG (FEI Company) operating at

Table 1. Codes and composition of the irradiated samples.

Sample	PA11 (wt%)	HNTs (wt%)	Radiation dose (kGy)
P0	100	0	0
P10	100	0	10
P20	100	0	20
P30	100	0	30
P50	100	0	50
P100	100	0	100
PH0	97	3	0
PH10	97	3	10
PH20	97	3	20
PH30	97	3	30
PH50	97	3	50
PH100	97	3	100

12.5 kV. The film sample was cryo-fractured and coated with a thin carbon layer and the observations of the fracture surface were made in the back-scattered electrons (BSE) mode.

Gel content. To determine the formed gel fraction in PA11 and PA11/HNTs nanocomposite during gamma radiation exposure, a solubility test was carried out on both the control and the irradiated samples in m-cresol. First, the samples were accurately weighed using an analytical balance to obtain the initial weight (Wi). Then, the weighted samples were immersed in m-cresol at 50°C under vacuum (Soxhlet apparatus) for 24 h. After the extraction process, the samples were washed and rinsed several times with ethanol to remove soluble materials and gels were collected by filtering through a fritted glass crucible. The weight of the insoluble materials (W_f) was obtained using an analytical balance. The gel fraction was calculated using equation (1).

$$Gel\ content = (W_f/W_i)*100\% \quad (1)$$

The reported values of the gel content were taken as the average of three measurements.

Fourier transform infrared spectroscopy. The modifications on the chemical structure induced by gamma irradiation were investigated by Fourier transform infrared (FTIR) spectroscopy. FTIR was performed on a spectrometer IFS 66 (Bruker). Spectra were obtained by collecting 64 scans between 400 and 4000 cm^{-1} with a resolution of 2 cm^{-1}.

Contact angle measurement. Contact angle measurements were obtained by depositing a liquid drop with controlled volume (2 μL) on the surface of the film. The contact angle (θ) measurements between the surface of the samples and two selected liquids (water and diiodomethane) with different dispersive (γ_L^D) and polar (γ_L^P) contributions were

performed using a KRÜSS Drop Shape Analyzer DSA30 goniometer apparatus. The dispersive (γ_S^D) and polar (γ_S^P) contributions to the surface energy of samples were calculated according to equation (2) using the Owens-Wendt model.[29]

$$\gamma_L \times (1 + \cos\theta) = 2\sqrt{\gamma_S^d \gamma_L^d} + 2\sqrt{\gamma_S^p \gamma_L^p} \quad (2)$$

where , γ_L^d and γ_L^p are known for the two different liquids used.

Three measurements were made at different location for each sample.

Spectrophotogoniometry. The evaluation of physical transparency is assessed through photometric measurements in the incidence plane by a GON 360° goniometer associated to a MAS 40 (Instrument Systems) spectrophotometer. The luminous source is localized at the normal (0°) of the sample and, in the opposite half-space with respect to the sample, the detector goes from −32.5° to 60° with a variable angular step (from 5° far from 0° to 0.5° around 0°). The measure can be integrated in all the incidence plane, giving a parameter of transmission of light when considered relative to the incident light (T). Three areas of each sample are characterized and the mean value is considered in this article.

Thermogravimetric analysis. Thermal stability of the irradiated samples was investigated by thermal gravimetric analysis (TGA) using a thermogravimetric analyzer SETSYS EVOLUTION (SETARAM). The specimens were heated to 600°C at a heating rate of 10°C/min. Measurements were carried out under nitrogen atmosphere with a flow rate of 20 ml/min on samples of approximately 20 mg. Values of $T_{5\%}$, $T_{50\%}$ and T_{mrd} were collected and these correspond to the decomposition temperature at 5% mass loss, the decomposition temperature at 50% mass loss and the temperature at maximum degradation rate determined at the maximum peak of DTG curve, respectively.

Crystallization behavior. The effect of gamma exposure on crystallization behavior of the irradiated samples was studied by differential scanning calorimetry (DSC) with a PYRIS DIAMOND DSC (Perkin Elmer Instruments) under nitrogen environment (20 ml/min). Samples of about 10 mg were heated from 30°C to 220°C at a rate of 10°C/min (first heating scan), equilibrated at 220°C for 5 min then cooled at 10°C/min to 30°C, equilibrated again at 30°C, then heated once more (second heating scan) always at 10°C/min. The measurements were performed from cooling and second heating scans, whereas, the first heating scan was made to eliminate the samples thermal history. Crystallization temperature (T_c), melting temperature (T_m) and melting enthalpy (ΔH_m) of the PA11 phase were determined. The degree of crystallinity (X_c) of the PA11 phase was calculated using equation (3):

$$Xc = \Delta H_m / \left(\Delta H_m^\circ \times w_t\right) \quad (3)$$

where ΔH_m is the melting enthalpy, ΔH°_m the melting enthalpy of the 100% crystalline polymer ($\Delta H^\circ_m = 206$ J/g[30]) and w_t the PA11 weight fraction in the composition.

Tensile test. Stress-strain analysis was carried out on ISO 527 1BA type tensile bars according to ISO 527 standard test procedure. An extensometer clip-on incremental (Zwick Roell) was used to measure accurately Young's modulus at a cross-head speed of 1 mm min^{-1}, whereas yield strength and elongation at break were determined at a speed of 20 mm min^{-1}. The measurements were conducted on a tensile machine Zwick Z010 (Zwick Roell) at environmental conditions. Prior to testing, the samples were stored at 23°C and 50% RH for 10 days, according to ISO 527 standard. At least 10 specimens of each formulation were tested and the average values were reported.

Experimental design

Factorial design was implemented to highlight main effects and interactions of both halloysite incorporation and gamma irradiation dose. Halloysite incorporation was set as the qualitative factor while gamma radiation dose was chosen as the quantitative one [0–100]. Surface energy and Young's modulus were selected as responses. The experimental design generates a polynomial equation of general form (equation (4)):

$$Y_i = b_0 + b_1X_1 + b_2X_2 + b_{12}X_1X_2 + b_{11}X_1^2 + b_{22}X_2^2 \quad (4)$$

where Y_i is the dependent variable (the response), b_0 the arithmetic mean response and b_i the estimated coefficient for the factor X_i. X_1 (halloysite incorporation) and X_2 (gamma radiation dose) represent the independent variables while the term X_1X_2 is representative of the interaction between the two factors. The polynomial equation is used in order to draw conclusions after considering the magnitude and sign of the coefficients.

Results and discussion

Morphology

First, a morphological investigation using SEM was carried out to confirm the nanocomposite morphology of the filled PA11. Figure 1 presents SEM micrographs of PA11/HNTs cryofractured film under various magnifications: ×2000 **(a)**, ×5000 **(b)**, ×20000 **(c)** and ×30000 **(d)**.

We can see from the different images that despite the presence of very small aggregates, corresponding in fact to the micronic particles resulting from the halloysite comminution process, HNTs are uniformly and individually dispersed at the nanoscale in the PA11 matrix thus forming a nanocomposite. Similar fine morphologies were described in the literature[19,20,31] and it is explained by the good affinity between halloysite nanotubes and polar PA11 matrix even without surface functionalization of the clay.

Structural investigation

The evolution of gel content for neat and filled PA11 with respect to gamma radiation dose is shown in Figure 2. The gel content corresponds to the crosslinking fraction formed in the amorphous region of the polymer, which is insoluble in m-cresol solvent.

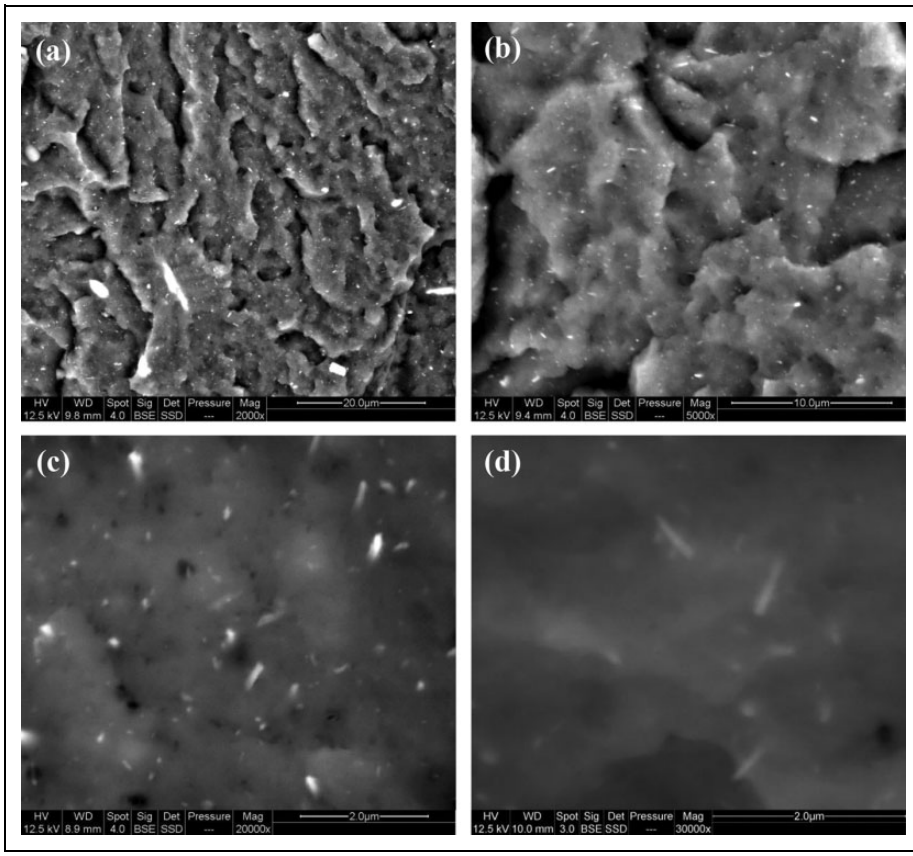

Figure 1. SEM micrographs of PA11/HNTs nanocomposite under various magnifications: ×2000 **(a)**, ×5000 **(b)**, ×20000 **(c)** and ×30000 **(d)**.

As seen in Figure 2, the dose of incipient gel is around 10 kGy for both neat PA11 and PA11/HNTs nanocomposite; a value which is much lower than that observed in gamma irradiation of PA6 (230 kGy).[28] Moreover, the maximum gel rate is obtained at 10 and 20 kGy for neat and filled PA11, respectively. After this, there is a slight decrease of the gel rate with increasing the dose, however being much higher for PA11/HNTs nanocomposite. It is known that the higher the gel content is, the higher the degree of crosslink density in amorphous regions becomes. This reduction of the gel rate does not mean any absence of crosslinking, but only that the rate of chain scission is faster than that of crosslinking. Indeed, if not enough material is available in the amorphous region to continue crosslinking, then the degradation of the surface of the lamellae surface take place with the same intensity. Therefore, chain scission predominates resulting in a decrease of the crosslinked part.[2] This is in contradiction with the effect of irradiation on some other polyamides like PA6 and PA6,6, where gel content was found to increase

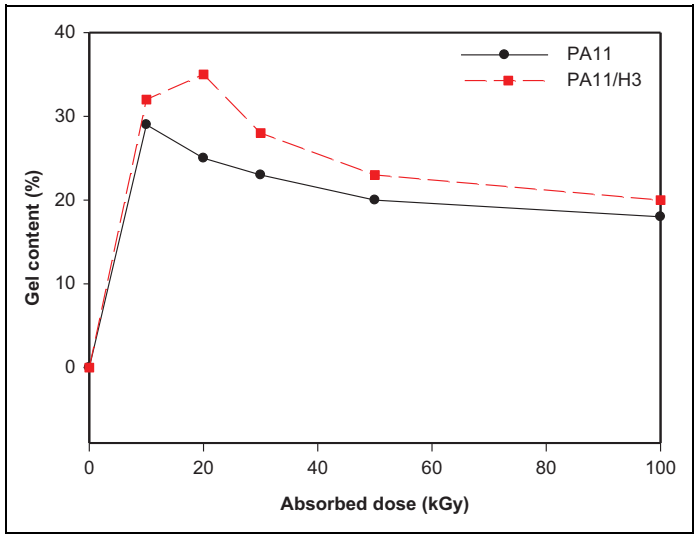

Figure 2. Evolution of the gel content of neat and filled PA11 as a function of the absorbed dose.

continuously with respect to radiation dose.[2,6] Nevertheless, it was also found that chain scission was predominating over crosslinking if irradiation of PA6 proceeded in air.[32] Indeed, in our study a relative low dose rate was used (1.92 kGy/h) generating a long time of exposure to radiation in oxidative atmosphere, so oxygen had enough time to attack the generated macro-radicals and thus favoring chain scission over crosslinking. Moreover, the process is also influenced by the melting temperature of polymer crystallites so that oxidation proceeds faster in PA11 compared to PA6 and 6,6.[2]

Regarding the effect of halloysite incorporation in PA11, it is worth noting that the γ-irradiated PA11 nanocomposite samples exhibit higher gel content compared to neat PA11. The difference in crosslinking or chain scission is due mainly to the presence of dissolved oxygen in the polymer. The barrier effect induced by HNTs hinders the penetration of oxygen into the matrix. Therefore, fresh oxygen cannot diffuse from the surface limiting further peroxidation which lead to the formation of more crosslinking rather than chain scission.

The main changes in the chemical structure of irradiated neat and filled PA11 were monitored by FTIR spectroscopy. FTIR spectra of neat PA11 before exposure and at 100 kGy in both the 1600–1800 cm^{-1} and the 2800–3500 cm^{-1} regions are shown in Figure 3(a) and (b), respectively. While FTIR spectra of filled PA11 samples before irradiation and at 100 kGy in the 1600–1800 cm^{-1} and the 2800–3500 cm^{-1} regions are shown in Figure 4(a) and (b), respectively.

As shown in Figure 3, there is no noticeable change in the position of the characteristics absorbance bands of PA11 at 100 kGy compared to the unexposed sample. Similar data were reported in the literature.[4] This was explained by the fact that there is no considerable radiolysis of side groups to be observed by FTIR.

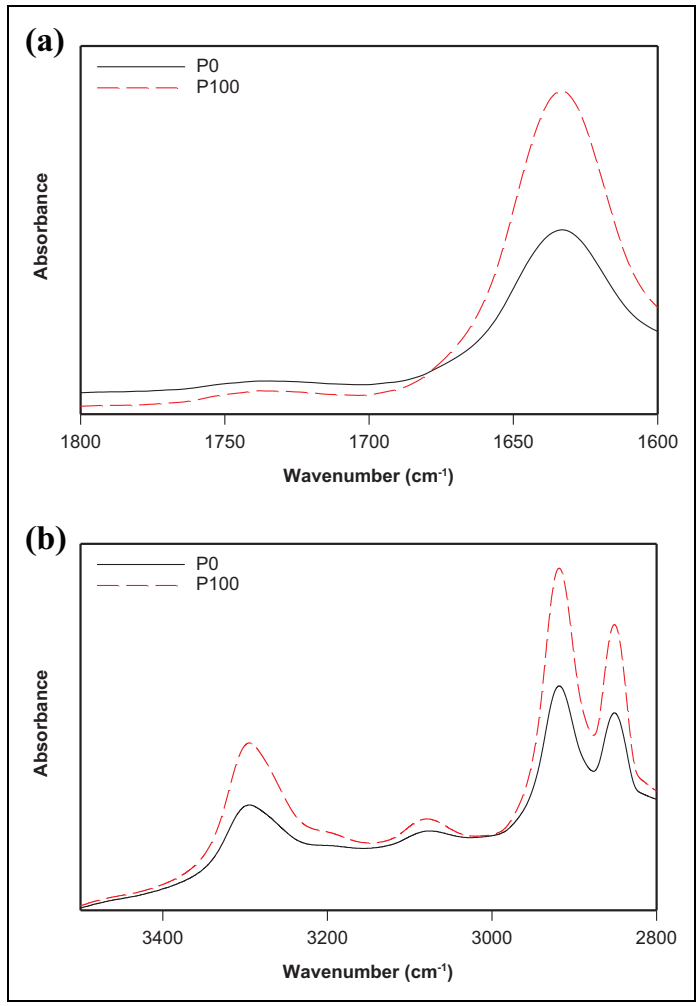

Figure 3. FTIR spectra of neat PA11 before exposure and at 100 kGy: **(a)** 1600–1800 cm^{-1} region **(b)** 2800–3500 cm^{-1} region.

However, the intensity of some absorbance bands increased. Indeed, as shown by Figure 3(a), the band at 1635 cm^{-1} assigned to the free and bonded C=O stretch (amide I) shows a higher intensity at 100 kGy. This is due to the formation of more carbonyl species during chain scission occurring at high radiation dose. Some others bands exhibit the same higher intensity in the course of γ-irradiation. These bands are located at 2852 and 2920 cm^{-1}, 3080 cm^{-1} and 3298 cm^{-1} corresponding to the symmetric and asymmetric CH_2, the doublet frequency of amide II and the hydrogen bonded NH stretch, respectively.[33] There too, this is explained by chain scission occurring at high irradiation dose.

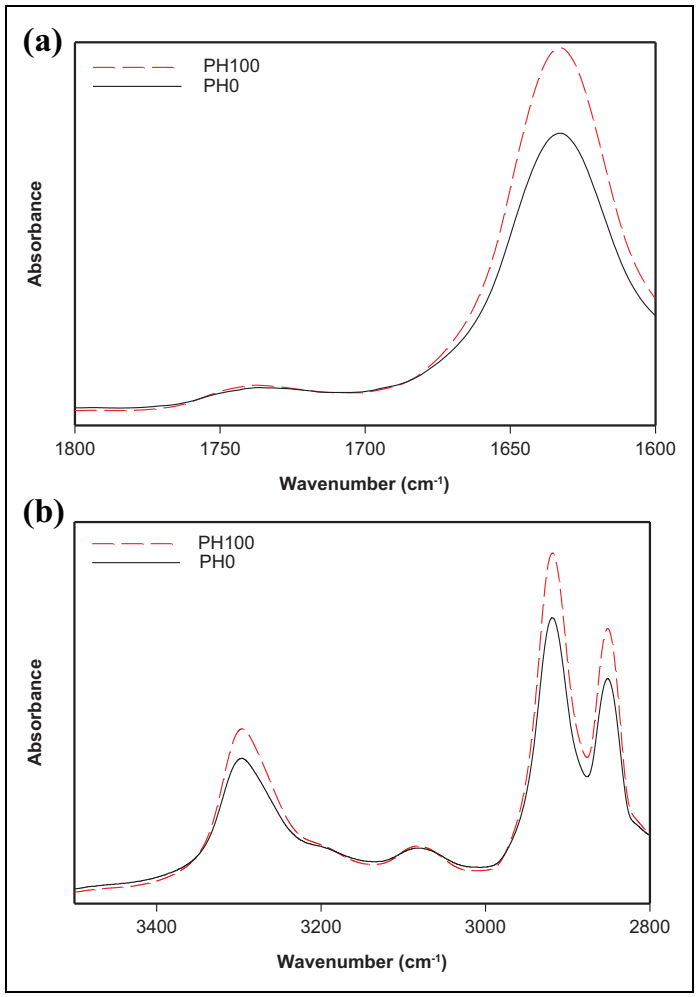

Figure 4. FTIR spectra of PA11/HNTs nanocomposite before exposure and at 100 kGy: **(a)** 1600–1800 cm^{-1} region **(b)** 2800–3500 cm^{-1} region.

Similar trend is observed for irradiated PA11/HNTs nanocomposite sample at 100 kGy compared to the one before exposure (see Figure 4). Nevertheless, the increase in the absorption intensity upon γ-irradiation is less important compared to the neat polymer, revealing the impact of HNTs which limits the effects of gamma irradiation of PA11.

The effect of gamma exposure on the surface chemistry of the irradiated samples was also investigated through the variation of surface energy. The values of the contact angle with water and diiodomethane and those of the resulting surface energy of the irradiated samples are listed in Table 2 as a function of radiation dose.

Table 2. Contact angle (°) with water and diiodomethane and surface energy (mJ/m^2) of the samples determined as a function of radiation dose.

Sample	Water Contact angle (°)	Diiodomethane Contact angle (°)	Surface energy (mJ/m^2)
P0	82.4	65.8	30.9 ± 0.9
P10	80.9	64.5	32.6 ± 0.8
P20	77.2	63	35.1 ± 1.1
P30	70.6	62.8	38.4 ± 1.1
P50	70.3	59.7	39.7 ± 1.2
P100	66.5	57.4	42.9 ± 1.3
PH0	83.5	60.2	32.5 ± 0.8
PH10	81.9	60.7	33.7 ± 1
PH20	81	60.3	34.4 ± 1.2
PH30	78.8	61.7	35.3 ± 1.3
PH50	77.4	61.1	36 ± 1.3
PH100	74.5	61.4	37.4 ± 1.2

From Table 2, it is observed that the water contact angle values of the irradiated samples decrease continuously with increasing the absorbed dose. This indicates a more hydrophilic surface of the irradiated samples due to the formation of polar groups like carbonyls. However, the correlation between the contact angle of diiodomethane and the absorbed dose is not clearly established. Indeed, a drop of the contact angle value with respect to the absorbed dose is observed for neat PA11. However, a slight increase of the contact angle value is noted for PA11/HNTs nanocomposites.

The values of surface energy increase with respect to the dose for both neat and filled PA11 samples, being more pronounced for neat PA11. This means the lower hydrophobicity of the materials due to the formation of hydrophilic species during gamma irradiation. Furthermore, we note that the surface energy increase of PA11/HNTs nanocomposite is lower than unfilled polymer. As example, at 100 kGy, P100 sample exhibits an increase in surface energy by 39% compared to control (P0), while PH100 sample possesses a surface energy superior by only 15% compared to the non-irradiated nanocomposite (PH0). This can be explained by the presence of HNTs that hinders the formation of hydrophilic compounds during gamma irradiation by barrier effect acting as anti-rad stabilizer.

The polynomial factorial equation for surface energy is equation (5):

$$Y_1 = 37.53 \pm 1.82X_1 + 0.69X_2 \pm 0.47X_1X_2 + 0.9{X_2}^2 \quad (5)$$

where Y_1 represents surface energy. The variability percentage (R^2) was found 0.983 indicating a good fit. The equation reveals that the sample composition has an antagonistic impact on surface energy (plus or minus sign). Indeed, the b_1 coefficient is positive for neat PA11 and negative in presence of HNTs. This can be explained by the fact that in presence of halloysite there is a less pronounced increase in surface energy

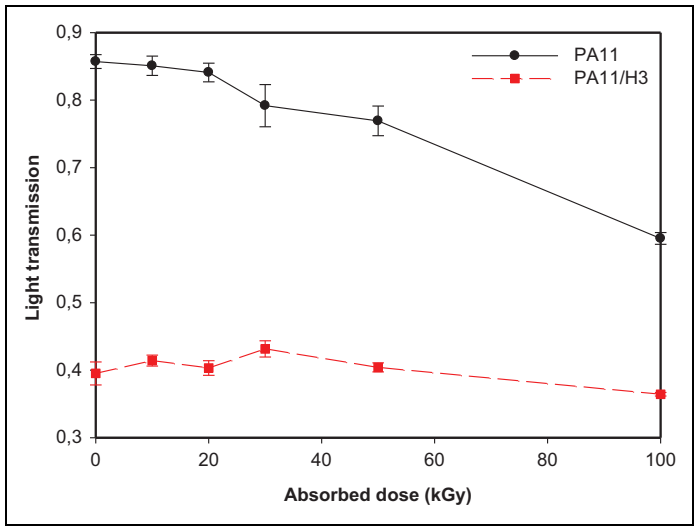

Figure 5. Evolution of the light transmission of neat and filled PA11 as function of the absorbed dose.

during gamma irradiation compared to the virgin polymer. Regarding the second factor, we have the confirmation of the positive impact of radiation dose on the evolution of surface energy.

The transparency of the irradiated films was evaluated by spectrophotogoniometry measurements. In this regard, Figure 5 shows the evolution of light transmission for both unfilled and filled PA11 as a function of the radiation dose.

One main observation that can be drawn from Figure 5, is the great difference between the transparency of neat PA11 films and those of PA11/HNTs nanocomposite. Indeed, PA11 films exhibit a much higher transparency compared to PA11/HNTs ones due to light scattering caused by HNTs nanoparticles, thus affecting the transparency of the samples. For PA11, increasing the dose leads to a significant increase in the film opacity. As a matter of fact, the light transmission decreases continuously with the absorbed dose, in particular above 20 kGy. The decrease in transparency is estimated to 30% at 100 kGy compared to the control value. This variation may result from the state of the surface or from the core of the material. The transparency loss is often due to light scattering caused by the presence of structural parts of the material having different refractive indexes resulting from changes in the microstructure such as crystallization. Although, the mechanism responsible for the transparency change in polyamides is still an unknown phenomenon. However, in the case of the irradiated nanocomposite films, no clear impact of gamma exposition is observed as the samples exhibit almost the same values of light transmission. This can be explained by the presence of HNTs that hinders the effect of gamma irradiation and consequently limits its impact on the transparency of PA11/HNTs films.

Table 3. Main thermal characteristic temperatures of the irradiated samples obtained by TGA and DSC.

Sample	$T_{5\%}$ (°C)	$T_{50\%}$ (°C)	T_{mrd} (°C)	T_{m1} (°C)	T_{m2} (°C)	T_c (°C)	X_c (%)
P0	421	463	472	192	192	165	22.7
P10	423	467	474	189	189	164	22
P20	419	464	471	188	188	163	21.2
P30	416	461	468	186	187	163	21.4
P50	408	455	463	184	185	163	20.9
P100	397	442	452	181	183	162	19.6
PH0	426	466	475	191	191	166	23.4
PH10	428	471	476	189	189	165	23.9
PH20	430	474	480	189	188	164	23.1
PH30	421	467	471	187	188	164	22.4
PH50	414	464	468	186	187	164	21.9
PH100	400	445	457	182	184	163	20.2

Thermal properties

The influence of gamma irradiation on thermal stability and crystallization behavior of the irradiated samples was investigated through TGA and DSC analyses, respectively and the obtained data are summarized in Table 3.

Regarding thermal stability, the results indicate that thermal stability of both neat and filled PA11 goes through two stages. First, an enhancement up to 10 and 20 kGy for neat and PA11/HNTs samples, respectively, then a constant decrease of thermal stability with respect to the absorbed dose. This is probably due to the formation of crosslinks at low irradiation dose which promotes thermal stability, then at higher doses, chain scission dominates creating low molecular weight species causing lower thermal stability.[34] Furthermore, nanocomposites samples show a superior thermal stability through the entire dose range. This higher stability of PA11/HNTs samples compared to neat matrix is because well dispersed HNTs act as an insulating barrier adding to the capacity of HNTs lumens to entrap degradation products.[25] Similar trend has been previously observed by other authors with layered silicates.[35] They reported that the resistance toward irradiation of nanocomposites are superior to those of neat polymers thanks to the dispersion at the nanoscale of the clay particles that hinders the penetration of gamma rays and decreases the formation of low molecular weight species generated by chain scission, thus stabilizing the nanocomposites.

Concerning the crystallization process, first it is observed that HNTs incorporation does not influence significantly the crystallization behavior of PA11 neither before nor after gamma irradiation exposure. From Table 3, it is seen a constant decrease of the melting temperature of the irradiated films with increasing irradiation dose. It decreased from 192°C for non-exposed PA11 (P0) to 183°C after irradiation at 100 kGy (P100). The decrease of T_m is attributed to the reduction of crystals size through gamma radiation in the solid state allowing crosslinking reactions to take place within the

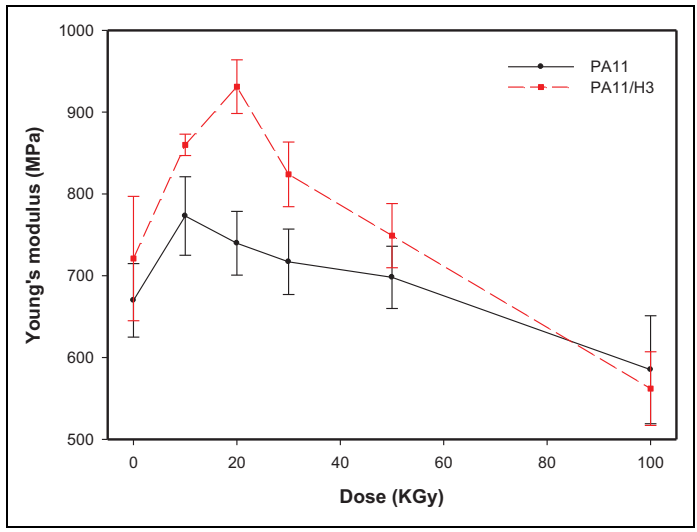

Figure 6. Evolution of the Young's modulus of filled and unfilled PA11 as function of the absorbed dose.

amorphous part of the polymer. In addition, crosslinking at the interface between crystalline and amorphous regions can result in the formation of a slightly altered crystalline phase which also leads to the drop of the melting temperature.[3] The results from DSC reveal furthermore that with increasing the absorbed dose, crystallization was progressively inhibited as the crystallization temperature T_c shifted to lower temperatures. The degree of crystallinity (Xc) slightly decreases with increasing the irradiation dose for all irradiated samples, the maximum being for P100 which exhibits a drop of almost 14% compared to non-irradiated material (P0). It is well known that chain scission as well as crosslinking reactions lead to loss in the degree of crystallinity. This can be explained by many reasons like the formation of some defects in the amorphous region which can block the crystallization from the melt. Moreover, reactions at the interface of amorphous and crystalline regions may make the latter slightly impaired.

Tensile properties

The effect of gamma irradiation on the tensile properties of the irradiated samples was investigated up to 100 kGy. The mechanical data are plotted as a function of the dose and shown in Figures 6 to 8 corresponding to Young's modulus, tensile strength and elongation at break, respectively for both neat PA11 and PA11/HNTs nanocomposite.

From Figure 6, it is observed that before irradiation, the nanocomposite sample exhibits a Young's modulus value higher by 12% than that of neat PA11 thanks to the natural stiffness of the nanoclay and also to its good dispersion in the PA11 matrix[19] (see Figure 1). After γ-irradiation exposure, an increase in the Young's modulus is observed for both neat and filled PA11 up to 10 and 20 kGy, respectively. The increase is

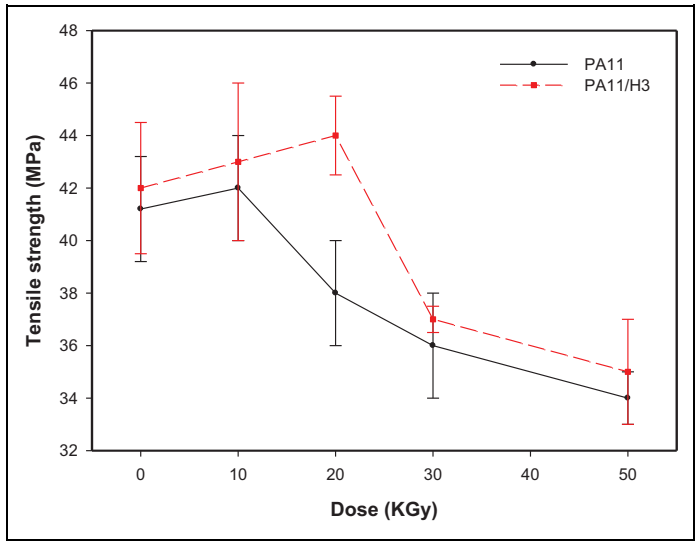

Figure 7. Evolution of the tensile strength of filled and unfilled PA11 as function of the absorbed dose.

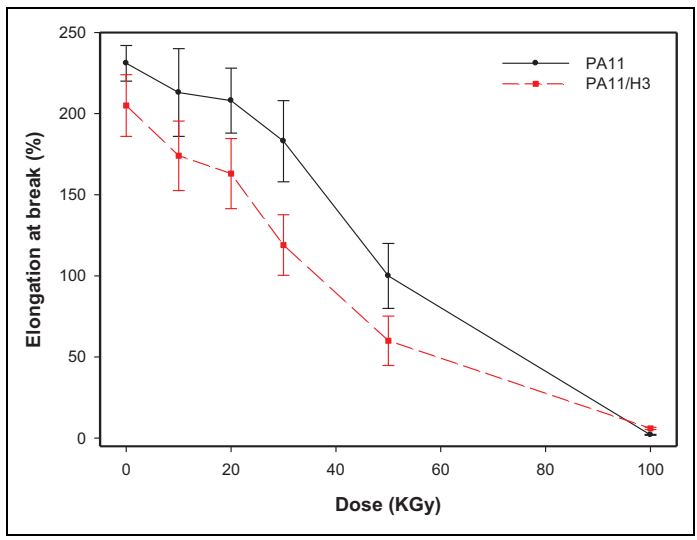

Figure 8. Evolution of the elongation at break of filled and unfilled PA11 as function of the absorbed dose.

estimated around 15.5 and 29% for neat and filled PA11, respectively. After that, a continuous decrease of Young's modulus is observed up to 100 kGy for both compositions. These phenomena are consistent with the gel content results and can be assumed

to the increased crosslinking of the amorphous phase at lower dose becoming more rigid so inducing an increase of the modulus.[36] While the drop of Young's modulus values for neat and filled PA11 observed beyond 10 and 20 kGy, respectively, can be explained by the predominant chain scission over crosslinking at higher irradiation dose that breaks down the long polymer chains into shorter ones. These shorter polymer chains possess a higher mobility and experience less restriction effects leading to more plastic deformation of the matrix.[37] Furthermore, crystallinity slightly decreased with the increase in irradiation dose (see Table 3) and so, a decrease in Young's modulus is expected.

On can also point out the fact that the increase in Young's modulus due to crosslinking is more important in presence of halloysite. In general, oxidative attacks result in peroxides and hydroperoxides formation, and therefore cause a decrease in the average molecular weight of the polymer through chain scission, and so to a decrease in the mechanical properties values.[38] Thus, at higher dose, HNTs can play a barrier role and so restrains the penetration of oxygen during the degradation, limiting the negative impact of gamma exposition on the mechanical characteristics of PA11.

Equation (6) represents the generated polynomial factorial equation for Young's modulus:

$$Y_2 = 762.99 \pm 37.35X_1 - 35.41X_2 \pm 12.47X_1X_2 - 32.28{X_2}^2 \quad (6)$$

where Y_2 represents Young's modulus. The variability percentage (R^2) was found 0.747 which indicates that the evolution of Young's modulus is rather random. As for surface energy, the equation points out the antagonistic effect of the filler presence (plus or minus sign). Nevertheless, this time the b_1 factor is negative for the neat polymer and positive in presence of halloysite. This is correlated to the fact that HNTs incorporation enhances Young's modulus compared to unfilled PA11, thus inducing a positive coefficient. Concerning the radiation dose factor, we remark a negative coefficient b_2. This is due to the overall decrease of Young's modulus values with increasing the dose.

Figure 7 displays the evolution of the tensile strength of the samples as function of irradiation dose, and similar trend with Young's modulus is observed. Indeed, tensile strength values reach a maximum then that optimum value decreases continuously with gamma dose. This can be due to the fact that tensile strength is a function of energy dissipation. Indeed, at lower dose, the crosslinks can dissipate the supplied energy, while at higher irradiation dose the crosslinks cannot dissipate further resulting in bonds breaking because the absorbed energy.[39]

Concerning elongation at break (Figure 8), a constant decrease is observed with respect to the irradiation dose. Nevertheless, the decrease is more pronounced beyond 20 kGy, which correspond to the maximum point of gel formation. The values of elongation at break of neat PA11 are higher compared to those of the filled one upon almost all exposure range, excepting at 100 kGy where neat and filled PA11 exhibit almost the same value. This is implying chain scission reactions upon gamma irradiation at higher doses[40] while at lower doses crosslinking and or branching could be the source of this drop of the elongation.[41]

Conclusions

The obtained results on gamma irradiation in air of neat PA11 and PA11 nanocomposite filled with 3 wt% of halloysite revealed the following conclusions:

1. A maximum of gel fraction is obtained at 10 and 20 kGy for neat and filled PA11, respectively. After that, the gel content slightly decreases with respect to irradiation dose.
2. The formation of hydrophilic species as evidenced through FTIR spectroscopy and confirmed by the higher surface energy of irradiated materials.
3. A loss of transparency after gamma exposure in the case of neat PA11 films unlike nanocomposite ones, which exhibit almost the same values of light transmission.
4. The thermal stability of both neat and filled PA11 goes through two stages. First, an enhancement up to 10 and 20 kGy for neat and PA11/HNTs samples, respectively, then a constant decrease of thermal stability with respect to the absorbed dose. This is due to the formation of crosslinks at low irradiation dose which promotes the thermal stability, then at higher doses, chain scission dominates lowering thermal stability.
5. The crystallization behavior of the irradiated samples is modified as both melting temperature and crystallization rate decrease with respect to the radiation dose due to chain scission and crosslinking reactions.
6. The tensile properties of neat and filled PA11 were affected through the variation of Young's modulus, tensile strength and elongation at break. An optimum irradiation dose was found for tensile properties, coincident with the dose for maximum gel content.
7. Enhanced properties were obtained for PA11/HNTs samples compared to neat PA11 indicating a more limited impact of gamma exposure thanks to the barrier effect of HNTs that hinders oxygen penetration and so the formation of low molecular species via chain scission.

Acknowledgments

The authors would thank EGIDE for its financial support through the Tassili program 13MDU891, to Jean-Jacques Flat from Arkema and the Algerian Company SOALKA for supplying PA11 resin and raw Algerian halloysite, respectively. The authors are also thankful to Benjamin Gallard of C2MA for his help during samples elaboration.

Funding

The author(s) received no financial support for the research, authorship, and/or publication of this article.

ORCID iD

Mohamed Sahnoune https://orcid.org/0000-0002-5301-8250

References

1. Elhady MA, Ghobashy MM and Mahmoud MA. Effect of gamma irradiation on the adhesive property and antibacterial activity of blend polymer (abietic acid-EVA). *Polym Polym Compos* 2021; 29: 138–147.
2. Porubská M, Szöllös O, Janigová I, et al. Crosslinking of polyamide-6 initiated by proton beam irradiation. *Radiat Phys Chem* 2017; 133: 52–57.
3. Dadbin S, Frounchi M and Goudarzi D. Electron beam induced crosslinking of nylon 6 with and without the presence of TAC. *Polym Degrad Stab* 2005; 89: 436–441.
4. Burillo G, Adem E, Muñoz E, et al. Electron beam irradiated polyamide-6 at different temperatures. *Radiat Phys Chem* 2013; 84: 140–144.
5. Gupta MC and Pandey RR. y-Irradiation of Nylon 6. *J Polym Sci A Polym Chem* 1988; 26: 491–502.
6. Sengupta R, Tikku VK, Somani AK, et al. Electron beam irradiated polyamide-6,6 films—I: Characterization by wide angle X-ray scattering and infrared spectroscopy. *Radiat Phys Chem* 2005; 72: 625–633.
7. Noura H, Amar B, Hocine D, et al. Effect of gamma irradiation aging on mechanical and thermal properties of alfa fiber-reinforced polypropylene composites: role of alfa fiber surface treatments. *J Thermoplast Compos Mater* 2018; 31: 598–615.
8. Abdel-Aziz M and Attia MK. The Physico-mechanical properties of γ-irradiated ethylene propylene diene rubber/high styrene butadiene rubber nanocomposites. *J Thermoplast Compos Mater* 2020. DOI : 10.1177/0892705720930800
9. Charlesby A. Effect of high-energy radiation on long-chain polymers. *Nature* 1953; 171: 167.
10. Lawton EJ, Bueche AM and Balwit JS. Irradiation of polymers by high-energy electrons. *Nature* 1953; 172: 76–77.
11. Deeley CW, Woodward AE and Sauer JA. Effect of irradiation on dynamic mechanical properties of 6–6 Nylon. *J Appl Phys* 1957; 28: 1124–1130.
12. Zimmerman J. Spectra of irradiated polyamides. *J Appl Polym Sci* 1959; 2: 181–185.
13. Zimmerman J. Degradation and crosslinking in irradiated polyamides and the effect of oxygen diffusion. *J Polym Sci* 1960; 46: 151–162.
14. Ueno K. The radiation crosslinking process and new products. *Int J Radiat Appl Instrumentation C Radiat Phys Chem* 1990; 35: 126–131.
15. Lyons BJ and Glover LC. Radiolytic crosslinking and chain scission in aliphatic and alkyl-aromatic polyamides. Part I. *Int J Radiat Appl Instrumentation C Radiat Phys Chem* 1990; 35: 139–147.
16. Joussein E, Petit S, Churchman J, et al. Halloysite clay minerals—a review. *Clay Miner* 2005; 40: 383–426.
17. Liu M, Jia Z, Jia D, et al. Recent advance in research on halloysite nanotubes-polymer nanocomposite. *Prog Polym Sci* 2014; 39: 1498–1525.
18. Handge UA, Hedicke-Höchstötter K and Altstädt V. Composites of polyamide 6 and silicate nanotubes of the mineral halloysite: influence of molecular weight on thermal, mechanical and rheological properties. *Polymer (Guildf)* 2010; 51: 2690–2699.
19. Sahnoune M, Kaci M, Taguet A, et al. Tribological and mechanical properties of polyamide-11/halloysite nanotube nanocomposites. *J Polym Eng* 2019; 39: 25–34.
20. Prashantha K, Lacrampe MFF and Krawczak P. Highly dispersed polyamide-11/halloysite nanocomposites: thermal, rheological, optical, dielectric, and mechanical properties. *J Appl Polym Sci* 2013; 130: 313–321.
21. Lecouvet B, Gutierrez JGG, Sclavons M, et al. Structure-property relationships in polyamide 12/halloysite nanotube nanocomposites. *Polym Degrad Stab* 2011; 96: 226–235.

22. Sahnoune M, Taguet A, Otazaghine B, et al. Fire retardancy effect of phosphorus-modified halloysite on polyamide-11 nanocomposites. *Polym Eng Sci* 2019; 59: 1–9.
23. Hao A, Wong I, Wu H, et al. Mechanical, thermal, and flame-retardant performance of polyamide 11-halloysite nanotube nanocomposites. *J Mater Sci* 2015; 50: 157–167.
24. Kennouche S, Le Moigne N, Kaci M, et al. Morphological characterization and thermal properties of compatibilized poly(3-hydroxybutyrate-co-3-hydroxyvalerate) (PHBV)/poly(-butylene succinate) (PBS)/halloysite ternary nanocomposites. *Eur Polym J* 2016; 75: 142–162.
25. Sahnoune M, Taguet A, Otazaghine B, et al. Inner surface modification of halloysite nanotubes and its influence on morphology and thermal properties of polystyrene/polyamide-11 blends. *Polym Int* 2017; 66: 300–312.
26. Sahnoune M, Taguet A, Otazaghine B, et al. Effects of functionalized halloysite on morphology and properties of polyamide-11/SEBS-g-MA blends. *Eur Polym J* 2017; 90: 418–430.
27. Hassan MM. Synergistic effect of montmorillonite-clay and gamma irradiation on the characterizations of waste polyamide copolymer and reclaimed rubber powder nanocomposites. *Compos B Eng* 2015; 79: 28–34.
28. Porubská M, Babić D, Janigová I, et al. The effect of gamma irradiation in air and inert atmosphere on structure and properties of unfilled or glass fibre-reinforced polyamide 6. *Polym Bull* 2016; 73: 1775–1794.
29. Owens DK and Wendt RC. Estimation of the surface free energy of polymers. *J Appl Polym Sci* 1969; 13: 1741–1747.
30. Mago G, Kalyon DM and Fisher FT. Nanocomposites of polyamide-11 and carbon nanostructures: development of microstructure and ultimate properties following solution processing. *J Polym Sci B Polym Phys* 2011; 49: 1311–1321.
31. Hedicke-Höchstötter K, Lim GT and Altstädt V. Novel polyamide nanocomposites based on silicate nanotubes of the mineral halloysite. *Compos Sci Technol* 2009; 69: 330–334.
32. Gupta MC and Pandey RR. y-Irradiation of Nylon 6. *J Polym Sci A Polym Chem* 1988; 26: 491–502.
33. Yu HH. Crystal phase transformations in nylon 11. *Mater Chem Phys* 1998; 56: 289–293.
34. Sengupta R, Sabharwal S, Bhowmick AK, et al. Thermogravimetric studies on Polyamide-6,6 modified by electron beam irradiation and by nanofillers. *Polym Degrad Stab* 2006; 91: 1311–1318.
35. Zaidi L, Bruzaud S, Kaci M, et al. The effects of gamma irradiation on the morphology and properties of polylactide/Cloisite 30B nanocomposites. *Polym Degrad Stab* 2013; 98: 348–355.
36. Adem E, Burillo G, del Castillo LF, et al. Polyamide-6: the effects on mechanical and physicochemical properties by electron beam irradiation at different temperatures. *Radiat Phys Chem* 2014; 97: 165–171.
37. Bee ST, Ratnam CT, Sin LT, et al. Effects of electron beam irradiation on the structural properties of polylactic acid/polyethylene blends. *Nucl Instruments Methods Phys Res B Beam Interact Mater Atoms* 2014; 334: 18–27.
38. Sengupta R, Sabharwal S, Tikku VK, et al. Effect of ambient-temperature and high-temperature electron-beam radiation on the structural, thermal, mechanical, and dynamic mechanical properties of injection-molded polyamide-6,6. *J Appl Polym Sci* 2006; 99: 1633–1644.
39. Sengupta R, Tikku VK, Somani AK, et al. Electron beam irradiated polyamide-6,6 films—II: mechanical and dynamic mechanical properties and water absorption behavior. *Radiat Phys Chem* 2005; 72: 751–757.

40. Dadbin S and Kheirkhah Y. Gamma irradiation of melt processed biomedical PDLLA/HAP nanocomposites. *Radiat Phys Chem* 2014; 97: 270–274.
41. Murray KA, Kennedy JE, McEvoy B, et al. Effects of gamma ray and electron beam irradiation on the mechanical, thermal, structural and physicochemical properties of poly (ether-block-amide) thermoplastic elastomers. *J Mech Behav Biomed Mater* 2012; 17: 252–268.